water

MDPI

Article

Selective Degradation of Organic Pollutants via Peroxymonosulfate-Based Electrochemical Advanced Oxidation Driven by Different Electrodes: Performance and Influencing Factors

Chen Zhang [1,2], Guang-Guo Ying [1,2], Yong Feng [1,2,3,*] and Jian-Liang Zhao [1,2,*]

[1] Guangdong Provincial Key Laboratory of Chemical Pollution and Environmental Safety, School of Environment, South China Normal University, Guangzhou 510006, China; 2023024814@m.scnu.edu.cn (C.Z.)
[2] MOE Key Laboratory of Theoretical Chemistry of Environment, School of Environment, South China Normal University, Guangzhou 510006, China
[3] Hunan Provincial Key Laboratory of Water Treatment Functional Materials, Hunan University of Arts and Science, Changde 415000, China
* Correspondence: fengy@scnu.edu.cn (Y.F.); jianliang.zhao@m.scnu.edu.cn (J.-L.Z.)

Abstract

Electrochemical advanced oxidation processes based on peroxymonosulfate (PMS-EAOPs) have shown great promise for eliminating organic pollutants from water. However, earlier research primarily concentrated on pollutant degradation at the cathode, with little attention given to the anode's role in PMS-EAOPs. In this work, we developed a PMS-EAOP system using nitrogen-doped carbon nanotubes (N-CNTs) as the electrocatalyst and examined the degradation of pollutants (acetamiprid (ATP) and sulfamethoxazole (SMX)) at both the cathode and anode. Our findings indicate that SMX was rapidly degraded at both electrodes, while ATP was effectively broken down only at the cathode, demonstrating the selective nature of PMS-EAOP. At a voltage of −2 V and 2.5 mM PMS, the pseudo-first-order rate constant (k_{obs}) for ATP at the cathode reached 0.122 min^{-1}, with over 92% removal within 30 min. In contrast, the anode exhibited high selectivity, removing ~75% of SMX (k_{obs} = 0.041 min^{-1}) while less than 20% of ATP was degraded. Analysis of reactive oxygen species showed that hydroxyl and sulfate radicals were produced and contributed to pollutant degradation at the cathode. In contrast, selective oxidation occurred at the anode, likely driven by direct electrolysis-induced nonradical oxidation responsible for the selective degradation. Phosphates and bicarbonates significantly inhibited the degradation of pollutants in the PMS-EAOP process (31.7–76.4%). In contrast, chloride ions exhibited an electrode-dependent effect, with the anode being less susceptible to interference from common water anions. Overall, this study highlights that while PMS-EAOP can selectively remove contaminants, the influence of water matrix components must be taken into account when treating real wastewater.

Keywords: PMS-EAOPs; selective oxidation; anode; electrochemical degradation

Check for updates

Academic Editor: Andreas N. Angelakis

Received: 2 January 2026
Revised: 24 January 2026
Accepted: 25 January 2026
Published: 28 January 2026

Copyright: © 2026 by the authors. Licensee MDPI, Basel, Switzerland. This article is an open access article distributed under the terms and conditions of the Creative Commons Attribution (CC BY) license.

1. Introduction

The diversified development of industry and the growing emphasis on healthcare have led to widespread concern over emerging contaminants (ECs) [1,2]. For example, the rapid expansion of the pharmaceutical and plastics industries in recent years has resulted in the release of ECs, such as pharmaceuticals and endocrine-disrupting compounds, into

groundwater and surface water [3,4]. ECs often exhibit chronic or acute toxicity and pose potential threats to aquatic ecosystems and human health, even at trace concentrations. Acetamiprid (ATP), a novel neonicotinoid insecticide structurally similar to nicotine, is a typical emerging contaminant. ATP not only exhibits high toxicity toward insects [5,6] but also has a strong affinity for mammalian nicotinic acetylcholine receptors [7], which accounts for its toxic effects on mammalian tissues. Due to its high solubility in water (~4.2 g/L) [8], ATP tends to accumulate in aquatic environments [9,10], leading to water pollution and potential bioaccumulation in aquatic organisms.

Over the past decade, various advanced treatment processes (AOPs) have been developed to remove ATP from water and wastewater [11]. A common feature of these AOPs is the generation of highly oxidizing reactive oxygen species (ROS) [12], such as hydroxyl radicals (·OH), sulfate radicals ($SO_4^{\bullet-}$), singlet oxygen ($^1O_2$), and high-valent metal-oxo species. These ROS can rapidly degrade ECs or even mineralize them into carbon dioxide and water. Although AOPs show great promise for treating ECs in aquatic environments, there are notable limitations with common AOPs in their practical application. For instance, significant efforts have been devoted to preparing and designing efficient nanofunctional materials for ROS generation via persulfate activation [13–15]. However, the practical use of nanopowder materials in water and wastewater treatment remains challenging due to difficulties in recovery and reuse.

Electrochemical advanced oxidation processes (EAOPs) represent a significant class of AOPs and have emerged as highly promising water treatment technologies for the removal of a broad range of organic pollutants. Their advantages include reduced chemical consumption, high efficiency, and suitability for long-term operation [16,17]. Based on the operating strategies, EAOPs are typically classified into three categories: anodic oxidation (AO), electro-Fenton (EF), and AO-EF [18]. The EF process relies on the cathodic electrogeneration of hydrogen peroxide (H_2O_2) and the external addition of Fe^{2+}. Since Fe^{2+} acts as a catalyst for radical formation via the Haber–Weiss mechanism, EF processes require strictly acidic conditions, typically within a narrow pH range of 2.0–4.0 [19]. Operating outside this range inevitably produces large amounts of iron sludge—as solid $Fe(OH)_3$ begins to precipitate significantly at pH values above 4.0—which substantially increases operational costs and may cause secondary pollution [19,20]. Recently, Lim et al. [21] demonstrated that adding peroxymonosulfate (PMS) instead of Fe^{2+} to the cathode side can significantly accelerate radical formation and pollutant degradation. Importantly, PMS-based EAOPs (PMS-EAOPs) avoid the need to adjust solution pH and prevent iron sludge formation, addressing major drawbacks of traditional EF processes. However, the authors only investigated pollutant degradation at the cathode side [21], leaving the reactivity of the anode side in PMS-EAOPs unexplored. Additionally, the impact of water matrices on this novel treatment technology remains unclear.

Nitrogen-doped carbon nanotubes (N-CNTs) have demonstrated superior performance in electrocatalysis due to their excellent conductivity and the presence of active nitrogen sites (e.g., pyridinic and graphitic N) that facilitate oxygen reduction and PMS activation [22–24]. However, challenges remain regarding their stability under high potentials and the complexity of large-scale fabrication [25]. To address these knowledge gaps, we developed a PMS-EAOP by preparing N-CNTs as the electrocatalyst for in situ H_2O_2 generation by reducing dissolved oxygen. The effects of PMS on both the cathode and anode sides, as well as the treatment performance of a PMS-EAOP, were evaluated using ATP and other common water contaminants, such as sulfamethoxazole (SMX), as target pollutants. The primary ROS involved were identified through electron paramagnetic resonance (EPR) tests and classical scavenging experiments. Additionally, the influence

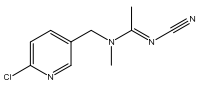
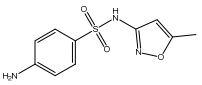
of common water constituents on PMS-EAOP performance was examined. Finally, the benefits and drawbacks of both anodic oxidation and cathodic oxidation were discussed.

2. Materials and Methods

2.1. Chemicals

All solutions were prepared with ultrapure water with a resistivity of greater than 18.0 MΩ·cm. Oxone ($KHSO_5 \cdot 1/2KHSO_4 \cdot 1/2K_2SO_4$), Nafion 117 solution, and H_2O_2 (3%) solution were purchased from Sigma-Aldrich (St. Louis, MO, USA). Sodium sulfate, sodium hydroxide, sulfuric acid, ATP, SMX, acetonitrile (HPLC grade, ≥99.9%), cerium sulfate, potassium iodide, sodium bicarbonate, DMPO (5,5-dimethyl-1-pyrroline-N-oxide, ≥97.0%), TEMP (2,2,6,6-tetra-methyl-piperidine), and urea were obtained from Aladdin (Shanghai, China). MWCNTs (≥98.0% C) were supplied by Nanotech Port Co., Ltd. (Shenzhen, China). The CAS numbers of these chemicals are detailed in Table S1. The physicochemical characteristics of ATP and SMX are listed in Table 1. River water samples were taken from the Pearl River in Guangzhou, China, and their properties are detailed in Table S2.

Table 1. Physicochemical properties of target pollutants.

Pollutant	Formula	Water Solubility	p*Ka*	Structure
ATP	$C_{10}H_{11}ClN_4$	2.95 g/L	4.6	
SMX	$C_{10}H_{11}N_3O_3S$	610 mg/L	1.6, 5.7	

2.2. Preparation of Electrodes and Characterization

MWCNT and urea were mixed in ethanol at specific weight ratios (1:1 and 1:2) under magnetic stirring overnight. The resulting suspension was dried at 60 °C and subsequently pyrolyzed in a tube furnace (KJ OTF-1200X, Hefei, China) under a nitrogen atmosphere. The temperature was increased to 800 °C at a rate of 5 °C/min and maintained for 2 h. After cooling to room temperature, N-CNT powders were obtained. N-CNT1 and N-CNT2 refer to the N-CNTs prepared with weight ratios of 1:1 and 1:2, respectively. The electrode loading was standardized based on area (1 cm^2). To prepare the N-CNT ink, 5 mg of N-CNT and 20 μL of Nafion 117 solution were dispersed in 2 mL of isopropanol, and the suspension was ultrasonicated for 2 h. The N-CNT working electrode was fabricated by drop-casting 0.2 mL of the prepared ink onto a carbon felt substrate with a geometric area of 1 cm × 1 cm × 0.2 cm (length × width × thickness). The electrode was then thoroughly dried in an oven at 60 °C prior to use.

A series of surface-sensitive instruments were employed to investigate the physical and chemical properties of electrocatalysts, as detailed in Text S1. Polarization curve measurements were conducted using a rotating disk electrode with a PINE AFMSRCE Research Instruments rotator assembly (Durham, NC, USA). Detailed procedures for the electrochemical analyses are provided in Text S2.

2.3. Electrocatalytic Degradation

All electrochemical experiments were conducted using a CHI660E electrochemical workstation (Chenhua Instruments, Shanghai, China) under laboratory conditions. A conventional two-compartment glass H-type electrolytic cell, separated by a Nafion 115 membrane, was used for all degradation experiments. The electrolytic cell has an inner diameter of 6 cm and a height of 7 cm for each chamber, with an inner diameter of 1.8 cm for the central connecting port. Unless otherwise specified, an Hg/Hg_2Cl_2 (saturated KCl

solution) electrode served as the reference electrode, and a platinum foil was employed as the counter electrode in the opposite chamber. The working electrode was the prepared N-CNT electrode. The fabricated carbon felt loaded with materials was secured using a stainless-steel clamp, followed by the installation of the reference and counter electrodes according to the schematic diagram shown in Figure 1. Unless otherwise specified, both chambers contained 100 mL of solution consisting of 50 mM sodium sulfate as the electrolyte, PMS (0–10 mM) as the oxidant, and 5 μM ATP/SMX as model pollutants at a pH of 3.2 ± 0.1. The aeration rate was maintained at 1 L/min. Aqueous samples were withdrawn from the chamber after the desired reaction time, filtered through PTFE filters, and immediately quenched with excess sodium thiosulfate.

$$\text{Degradation percentage} = \frac{C_t - C_0}{C_t} \times 100\% \quad (1)$$

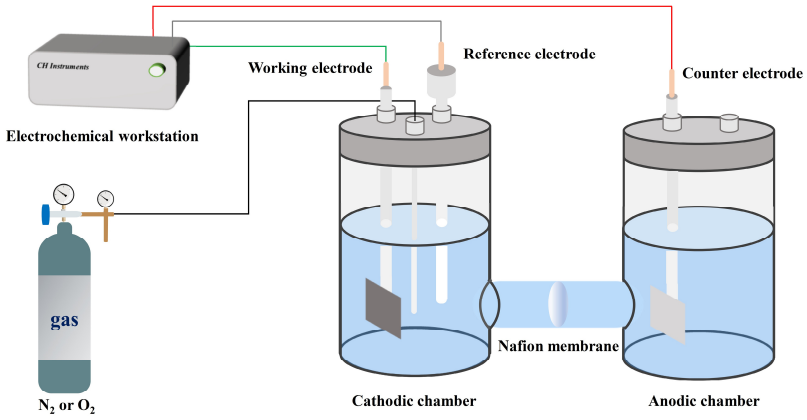


Figure 1. Schematic diagram for the electrocatalytic device.

The degradation percentage of the pollutant was calculated using Equation (1), where C_0 is the initial concentration of the pollutant and C_t is the concentration at reaction time t. The degradation of ATP was modeled using pseudo-first-order kinetics (Equation (2)).

$$-\ln\frac{C_t}{C_0} = k_{obs}dt \quad (2)$$

where k_{obs} is the pseudo-first-order rate constant (min^{-1}).

2.4. Chemical Analysis

Quantitative analyses of organic compounds, including ATP and SMX, were performed using a high-performance liquid chromatography system (Agilent 1260 Infinity II, Santa Clara, CA, USA) equipped with a reverse-phase C18 column (Agilent Eclipse XDB-C18, 2.7 μm particle size, 2.1 mm × 100 mm). For more details, please refer to Text S3. The concentrations of PMS and H_2O_2 were measured using the potassium iodide method and the ceric sulfate method, respectively (Texts S4 and S5). The detection of ROS was performed using an ESR5000 electron paramagnetic resonance spectrometer (Bruker, Karlsruhe, Germany). Detailed analytical parameters are provided in Text S6.

3. Results and Discussion

3.1. Characterization of Catalysts and Working Electrodes

The XPS spectra of CNTs and N-CNTs (N-CNT2) were recorded to analyze the surface elemental composition (Figure S1). The results indicate that treatment with urea increased the nitrogen content of CNTs, with N-CNT2 exhibiting the highest nitrogen content (1.27%)

(Figure 2a). Further analysis of the high-resolution N 1s XPS spectrum of N-CNT2 revealed that the nitrogen was primarily composed of pyridinic N, pyrrolic N, graphitic N, and oxidized N [26], with pyridinic N being the most abundant species (Figure S1). Pyridinic N is known to have a strong affinity for oxygen adsorption [27], which facilitates O–O bond cleavage and electron transfer. The morphology of raw and N-CNT2-modified carbon felts was examined using scanning electron microscopy. Compared to the smooth surface of raw carbon felt (Figure 2b), the modified felt exhibited a much rougher texture, with distinct particles present on the surfaces (Figure 2c). At higher magnification, characteristic tubular structure of CNTs was observed (Figure 2d), confirming the successful loading of N-CNT2 onto the carbon felt.

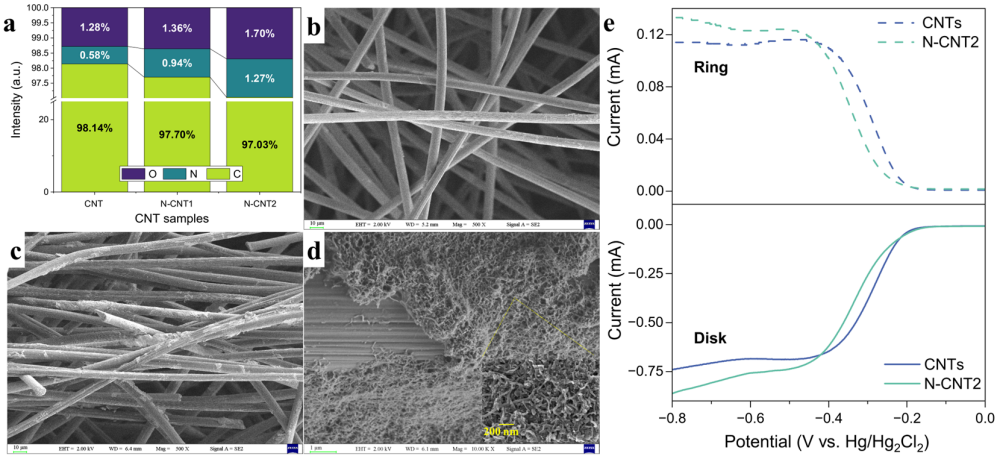


Figure 2. (**a**) Elemental percentages of CNT samples, scanning electron microscopy images of (**b**) carbon felt and (**c**,**d**) N-CNT2 modified carbon felts, and (**e**) polarization curves at 1600 rpm (solid lines) and simultaneous H_2O_2 detection currents at the ring electrode (dashed lines).

The oxygen reduction reactivity of N-CNTs was investigated through electrochemical characterization. The current associated with oxygen reduction was measured using a disk electrode, while the current for H_2O_2 oxidation was measured on a ring electrode. According to the polarization curves (Figure 2e), N-CNT2 exhibited a higher current compared to raw CNTs. Additionally, the ring current data revealed that H_2O_2 formation performance with N-CNT2 was significantly superior to that with CNTs. Consistent with previous findings [21], these results suggest that N-CNTs may exhibit enhanced reactivity in the EF process for pollutant degradation. To further elucidate this, the electrochemically active surface area (ECSA), normalized by the geometric area of the electrode, was evaluated as a critical metric for electrode performance. Figure S2 was obtained by fitting the electrochemical double-layer capacitance (Cdl) derived from cyclic voltammetry curves. To determine the Cdl values, the cyclic voltammetry measurements were conducted at various scan rates (10, 20, 40, 60, 80, 120, 160, and 200 mV/s) within the non-Faradaic potential region. The Cdl value of N-CNTs (N-CNT2, 6.530×10^{-4} mF cm^{-2}) was 6.0% higher than that of CNTs (6.164×10^{-4} mF cm^{-2}), indicating a notable increase in the availability of active sites, which is a key factor in enhancing electrocatalytic efficiency. The material with the highest nitrogen content, N-CNT2, was selected to fabricate the working electrode and utilized in the following experiments.

3.2. Electrocatalytic Oxidation

The effects of CNT catalysts and nitrogen doping on the treatment performance were investigated (Figure 3a). When raw carbon felt was used as the cathode, ATP degradation proceeded with slow kinetics (only 48.3% was degraded after 20 min), likely due to the formation of radicals via the electro-activation of PMS [28]. In contrast, when CNT-modified

carbon felt was used as the cathode, ATP degradation occurred much more rapidly (more than 80% was degraded after 20 min), demonstrating the catalytic effect of CNTs. Furthermore, an additional increase in degradation kinetics was observed when N-CNTs were used as the electrocatalyst instead of raw CNTs (around 92% was degraded after 20 min). As shown in Figure 3b, at a constant PMS concentration (2.5 mM) without the application of electricity, the concentration of ATP remained nearly unchanged, confirming ATP's resistance to PMS oxidation and highlighting the critical role of electricity. When a voltage of −2 V was applied, ATP degradation occurred rapidly, with nearly complete removal after only 30 min of reaction. In the absence of PMS, ATP was degraded at a much slower rate, with an overall removal percentage of less than 60%. These results indicate a strong synergistic effect between PMS and electrocatalysis in the degradation of ATP.

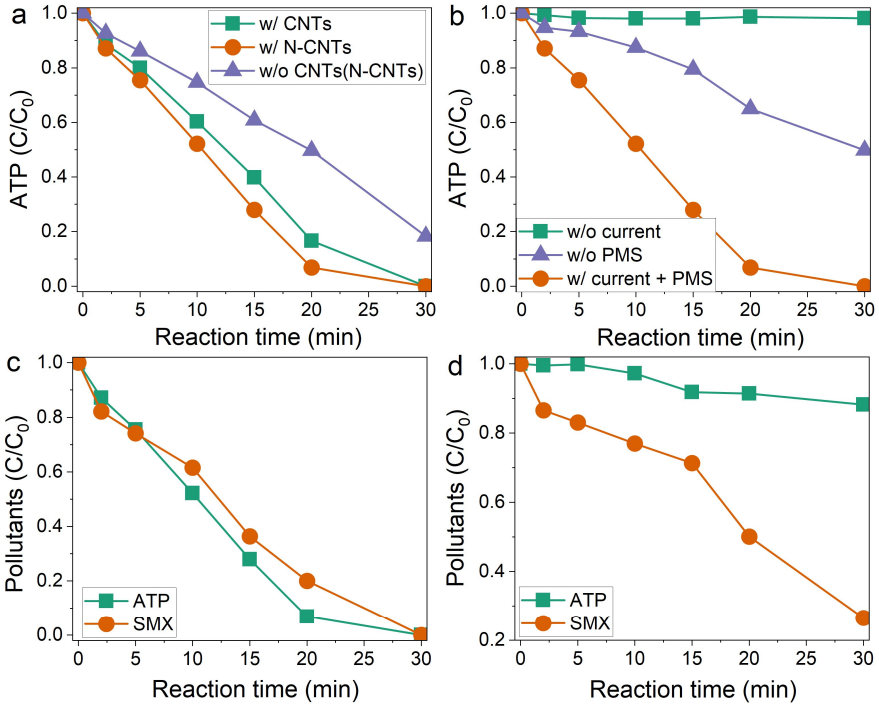


Figure 3. Effects of (**a**) catalysts, (**b**) current, and (**b**) PMS on the cathode degradation of ATP by PMS-EAOP; simultaneous degradation of pollutants in (**c**) cathode and (**d**) anode sides of PMS-EAOP. Conditions: voltage = −2 V, [PMS] = 2.5 mM, [ATP] = 5 μM, (**c**,**d**) [SMX] = 5 μM, and initial pH = 3.2 ± 0.1.

In addition to ATP, SMX was used as another target pollutant to evaluate the treatment performance of the electrocatalytic system. Similar to ATP, SMX was rapidly degraded on the cathode side (Figure 3c). To maximize the utilization of electrical energy, experiments were conducted to degrade the target pollutants on the anode side. However, only SMX was efficiently degraded in this region (Figure 3d). The overall removal percentage of ATP was less than 20%, which was significantly lower than that of SMX (~75%). This selectivity is not coincidental but is determined by the intrinsic molecular orbital energies of the contaminants. The SMX molecule contains electron-rich functional groups, namely the aniline moiety and the isoxazole ring, with an oxidation peak potential of approximately 0.72 V (vs. Ag/AgCl), which lowers its ionization potential and facilitates direct electron transfer at the anode surface [29]. In contrast, ATP incorporates strong electron-withdrawing groups, including the cyano group (-CN) and the chlorinated pyridine ring, which substantially raise the oxidation potential of the molecule and thereby enhance its resistance to direct anodic oxidation [30]. To examine the degradation mechanisms occurring at the cathode and anode, ATP and SMX were selected as the respective target pollutants.

3.3. Effects of Influencing Factors

The effects of key experimental parameters, including PMS concentration, applied voltage, solution pH, and rotation speed on electrocatalytic reactivity, were examined. Increasing the PMS concentration from 1 mM to 10 mM significantly accelerated ATP degradation at the cathode (Figure 4a). The degradation of ATP followed a pseudo-first-order rate law (Figure S3), and the pseudo-first-order rate constant at 10 mM PMS was more than 51 times greater than that at 1 mM. However, it is noteworthy that excessively high PMS dosages may introduce a 'scavenging effect' where PMS reacts with the generated $SO_4^{\bullet-}$ and ·OH to form $SO_5^{\bullet-}$ radicals, which possess significantly lower oxidation potentials. Additionally, high concentrations can trigger ineffective self-decomposition of the oxidant ($HSO_5^- \rightarrow 2SO_4^{2-} + O_2 + 2H^+$), potentially reducing the oxidant utilization efficiency and increasing treatment costs in practical applications. At the anode, however, the increase in the PMS dosage resulted in only a marginal enhancement, as illustrated in Figure 4b.

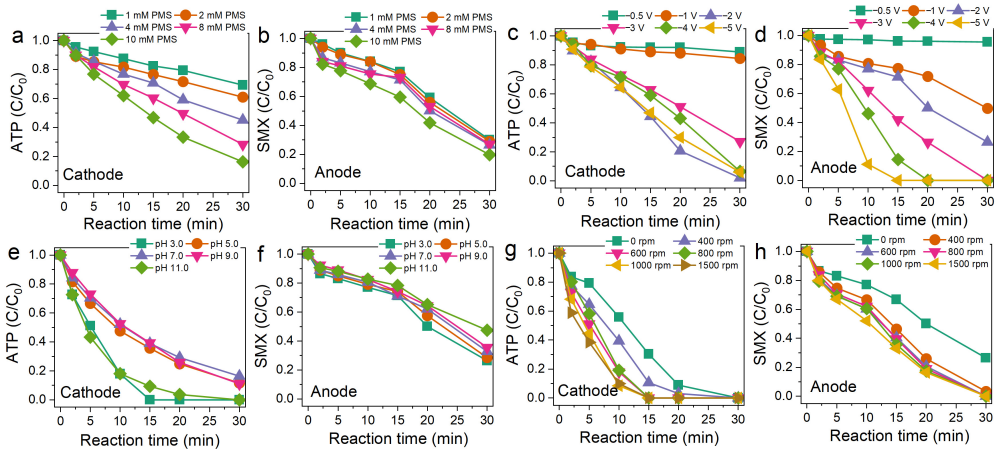


Figure 4. Effects of (**a**,**b**) PMS, (**c**,**d**) voltage, (**e**,**f**) solution pH values, and (**g**,**h**) rotation speed on the degradation of ACMP and SMX by PMS-EAOP. Conditions: (**a**,**b**,**e**–**h**) voltage = −2 V, (**c**–**h**) [PMS] = 2.5 mM, [ATP] = 5 μM, [SMX] = 5 μM, and (**a**–**d**,**g**,**h**) initial pH = 3.2 ± 0.1.

The results in Figure 4c,d demonstrate that electricity plays a crucial role in pollutant degradation. To determine the optimal conditions, the effect of the voltage applied to the electrocatalytic reactor was investigated. It was observed that ATP degradation proceeded with slow kinetics at low voltages (≤−1 V) (Figure 4c). A significantly faster degradation of ATP occurred when the voltage was increased to −2 V, while further increases in voltage slowed the degradation process. These findings indicate that the optimal voltage value for pollutant degradation at the cathode side is −2 V. At the anode, elevating the voltage from −0.5 V to −5 V significantly enhanced the degradation of SMX. This enhancement was more substantial compared to that observed at the cathode (Figure 4d), indicating that the treatment efficacy at the anode is more sensitive to variations in the applied voltage.

The solution pH is a crucial factor influencing the speciation of reactants (pollutants and PMS) and the surface properties of electrodes. Investigation of this parameter revealed that both acidic and basic conditions (pH 3.0 and 11.0) were more favorable for ATP degradation than circumneutral pH conditions (5.0–9.0) (Figure 4e). Under basic conditions, the self-decomposition of PMS can generate $^1O_2$ [31], a species capable of degrading ATP [32]. Therefore, the efficient ATP degradation observed at pH 11.0 is likely partly due to the formation of $^1O_2$. In addition, $SO_4^{\bullet-}$ is converted to ·OH under strongly alkaline conditions [33]. These reactive species work synergistically to accelerate the degradation of ATP. Conversely, PMS activation at acidic pH (~3.0) is more challenging because high concentrations of H^+ ions stabilize PMS, inhibiting its activation [34]. The efficient ATP

degradation at pH 3.0 is probably attributable to the enhanced electrocatalytic reactivity of N-CNTs [21]. At the anode, the pH of the solution exhibited a minimal influence on the degradation of SMX; however, acidic conditions were generally found to be more favorable for the degradation of pollutants (Figure 4f).

The rotation speed of the reactor influences the mass transfer of reactants and, consequently, the degradation of pollutants. Within the rotation speed range of 200–600 rpm, the degradation of ATP showed a positive correlation with speed (Figure 4g). This indicates that mass transfer was the rate-determining step in the electrocatalytic reactor. However, further increases in rotation speed did not significantly accelerate degradation, suggesting that the system became kinetically controlled at speeds above 600 rpm. A comparable phenomenon was observed in the degradation of SMX at the anode side (Figure 4h). Similar situations were reported by Nhu et al. [35]. Based on these results, the rotation speed for subsequent experiments was fixed at 600 rpm.

Literature documenting the treatment of ATP or SMX using PMS-EAOPs is relatively scarce. Therefore, we conducted a comparative analysis of the treatment efficiencies of various PMS-EAOPs applied to organic pollutants exhibiting similar reaction rate constants with hydroxyl radicals, approximately 10^9 M^{-1} s^{-1} (Table S3 [36–38]). The findings indicate that, within these studies, N-CNT2 demonstrates the highest reactivity for pollutant degradation, as evidenced by the maximum observed rate constant of 0.123 min^{-1}.

3.4. Identification of ROS

To investigate ROS, the EPR spectra of the reaction media from both the cathode and anode sides were analyzed. Previous studies have shown that ·OH, $SO_4^{\bullet-}$, and $^1O_2$ can be generated during the activation of PMS [39,40]. Therefore, EPR tests were conducted to detect these species. Using DMPO as the spin-trapping agent, a characteristic four-line EPR signal with a 1:2:2:1 quartet ($\alpha N = \alpha H = 1.48$ mT) was observed in both electrode cells (Figure 5a,b). This signal corresponds to the formation of DMPO-·OH adducts [41], indicating the presence of ·OH. Notably, quantitative analysis through baseline correction and integration of the EPR signals revealed that the ·OH signal intensity at the cathode was approximately 4.8 times higher than that at the anode. This 4.8-fold difference confirms substantially greater ·OH generation at the cathode, which is consistent with the efficient cathodic activation of PMS observed in this system. Additionally, signals corresponding to DMPO-$SO_4^{\bullet-}$ adducts were detected in the cathode cell (Figure 5a), indicating the formation of $SO_4^{\bullet-}$. The production of singlet oxygen was also examined using EPR with 2,2,6,6-tetramethyl-piperidine (TEMP) as the spin-trapping agent. However, the distinctive signal for this species was very faint (Figure S4), indicating that the generation of singlet oxygen at both the cathode and anode was minimal.

Both ·OH ($k = 5.5 \times 10^{10}$ M^{-1} s^{-1}) [42] and $SO_4^{\bullet-}$ ($k = (1.1 \pm 0.6) \times 10^9$ M^{-1} s^{-1}) [43] react rapidly with ATP. Since these ROS were confirmed to be formed, classical quenching tests using MeOH and TBA were conducted to evaluate their contributions to pollutant degradation. MeOH reacts rapidly with both ·OH ($k_{\bullet OH} = 9.7 \times 10^8$ M^{-1} s^{-1}) [44] and $SO_4^{\bullet-}$ ($k_{SO_4^{\bullet-}} = 1.0 \times 10^7$ M^{-1} s^{-1}) [45], while TBA is reactive only toward ·OH ($k_{\bullet OH} = 3.3 \times 10^9$ M^{-1} s^{-1}, $k_{SO_4^{\bullet-}} = 4.1$–$9.0 \times 10^5$ M^{-1} s^{-1}) [44,46]. The combined use of MeOH and TBA allows differentiation of the contributions of these species. At the cathode side, the overall degradation rate of ATP decreased significantly from nearly 100% to 4.6% and 13.6% in the presence of 0.5 M MeOH and 0.5 M TBA (Figure 5c), respectively, suggesting that ·OH is mainly responsible for the degradation.

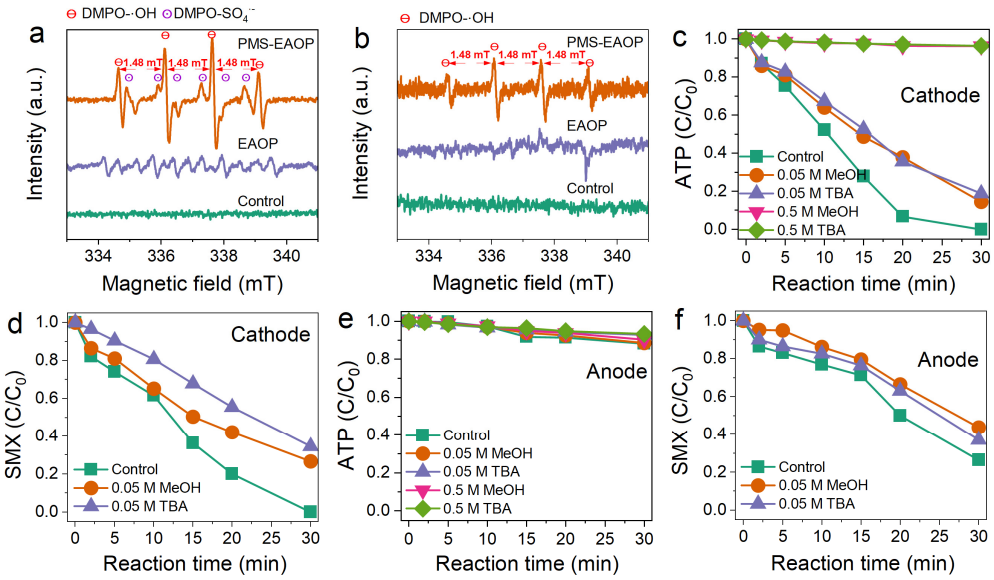


Figure 5. EPR spectra of reaction solutions in the (**a**) cathode and (**b**) anode cells of PMS-EAOP and effects of radical scavengers on the degradation of pollutant in the (**c**,**d**) cathode and (**e**,**f**) anode sides of PMS-EAOP. Conditions: voltage = −2 V, [PMS] = 2.5 mM, (**a**,**b**) [DMPO] = 50 mM, (**c**,**e**) [ATP] = 5 μM, (**d**,**f**) [SMX] = 5 μM, and initial pH = 3.2 ± 0.1.

Meanwhile, compared to MeOH, TBA has a higher second-order rate constant with ·OH, but exhibits a relatively weaker inhibitory effect than MeOH. This observation aligns with the EPR results and suggests that $SO_4^{\bullet-}$ also plays a role in the degradation of ATP. Pronounced inhibitory effects of MeOH and TBA on the degradation of SMX were also observed (Figure 5d), further corroborating the critical role of radical species. Nevertheless, over 60% of SMX degradation persisted despite the presence of 0.05 M MeOH or TBA, indicating the contribution of a non-radical oxidation pathway.

At the anode, the presence of radical scavengers did not significantly influence the degradation of ATP, as this compound remained undegraded (Figure 5e). Meanwhile, the presence of either MeOH or TBA slowed down the degradation of SMX, with no significant difference observed between the effects of MeOH and TBA. This suggests that ·OH was formed and played a role in the degradation process, while the involvement of $SO_4^{\bullet-}$ was minimal. However, the inhibitory effect of these alcohols was notably weaker compared to that seen on the cathode side (Figure 5d); over 65.0% and 60.9% of SMX were still degraded in the presence of 0.5 M MeOH and 0.5 M TBA (Figure 5f), respectively. These results indicate that ATP degradation at the anode primarily occurs through a non-radical mechanism, although ·OH radicals also contribute.

The overpotential required for oxygen evolution on platinum anodes is relatively low (approximately 1.6 V vs. SHE in 0.5 M H_2SO_4) [47], suggesting that direct electrolysis likely drives ATP degradation. According to our recent study, SMX donates electrons more easily than ATP [48], which accounts for the selective degradation of SMX (Figure 3d). The formation of ·OH at the anode can be attributed to water oxidation occurring on the electrode surface (Equation (3)) [47].

$$H_2O \rightarrow H^+ + \bullet OH + e^- \quad (3)$$

3.5. Mechanisms for ROS Generation at the Cathode Side

Although the role of ·OH in pollutant degradation has been confirmed, the exact process by which these ROS are formed is still not fully understood. Earlier research has indicated that ROS can be produced through the cathodic electroactivation of PMS

(Equations (4) and (5)) [49]. However, this mechanism alone does not account for the notable influence of the reactor's rotation speed. To gain deeper insight into the mechanism, linear sweep voltammetry was performed. The findings revealed that purging with N_2 had only a minimal impact on current changes (Figure 6a), whereas purging with O_2 significantly increased the current (Figure 6b). Based on the well-known oxygen reduction reaction pathway [50], O_2 is reduced at the cathode to H_2O_2 through a two-electron transfer process (Equations (6) and (7)). The crucial role of O_2 implies that its reduction product, H_2O_2, likely participates in generating the ROS responsible for pollutant degradation. To test this idea, the effect of O_2 and N_2 purging on H_2O_2 production was examined. Results showed that H_2O_2 levels were much higher under O_2 purging compared to N_2 purging (Figure 6c). By reacting with H_2O_2, PMS is activated to produce $SO_4^{\bullet-}$ (Equation (8)) [21], which explains the importance of O_2 and the impact of rotation speed on the degradation of ATP. These $SO_4^{\bullet-}$ are highly unstable in water and convert into ·OH through reactions with H_2O or OH^- (Equation (9)) [41]. Furthermore, the decomposition of PMS in the cathode cell was studied. The data demonstrated that PMS decomposed quickly even without the presence of target pollutants (Figure 6d), supporting the idea that radical-driven degradation pathways are involved. The slight enhancement of PMS decomposition by ATP is probably due to direct electron transfer between them, causing minor ATP degradation by PMS alone (Figure 3b).

$$HSO_5^- + e^- \rightarrow SO_4^{\bullet-} + OH^- \quad (4)$$

$$HSO_5^- + e^- \rightarrow SO_4^{2-} + \bullet OH \quad (5)$$

$$O_2 + H_2O + e^- \rightarrow *OOH + OH^- \quad (6)$$

$$*OOH + e^- \rightarrow HO_2^- \quad (7)$$

$$HSO_5^- + HO_2^- \rightarrow SO_4^{\bullet-} + O_2^{\bullet-} + H_2O \quad (8)$$

$$SO_4^{\bullet-} + OH^-/H_2O \rightarrow SO_4^{2-} + \bullet OH \quad (9)$$

The impact of common anions in surface water on PMS-EAOP was investigated by examining the degradation kinetics of pollutants. The concentrations of these tested anions generally fell within their actual environmental concentration ranges. When the concentrations of phosphates, bicarbonates, and chloride ions increased from 0 to 5 mM, the k_{obs} of ATP values in the cathode side decreased significantly from 0.123 to 0.029, 0.042, and 0.009 min^{-1} (Figure 7a–c), respectively. Meanwhile, the k_{obs} of SMX values in the anode side decreased from 0.041 to 0.028 and 0.024 min^{-1} when the concentrations of phosphates and bicarbonates increased from 0 to 5 mM (Figure 7d,e). Unlike the pronounced inhibitory impact of chloride ions on ATP degradation, the presence of this anion marginally enhanced the degradation of SMX at the anode. According to their dissociation constants (Table S4 [51–53]) [53], phosphates and bicarbonates mainly exited in the form of $H_2PO_4^-$ (>80%) and H_2CO_3, respectively. The second-order rate constant between $H_2PO_4^-$ and ·OH is 2×10^4 M^{-1} s^{-1} [54], and that between H_2CO_3 and ·OH is only 7×10^4 M^{-1} s^{-1} (5 °C) [51]. Since these values are less than 1/105 of the rate constant of ATP with ·OH (5.5×10^{10} M^{-1} s^{-1}) [42], the scavenging capacity of both phosphates and bicarbonates toward ·OH is expected to be negligible. The observed negative effects of phosphates and bicarbonates on both electrodes are likely due to their competitive adsorption with other reactants for active sites on the electrode surface. Chloride ions are reactive toward ·OH (4.3×10^9 M^{-1} s^{-1}) [45] and PMS (2.06×10^{-3} M^{-1} s^{-1}) [55], producing reactive chlorine species such as chloride radicals and hypochlorous acid. Although these chlorine species are less oxidative than ·OH, they are more selective. Previous studies have reported that high levels of chloride ions promoted the degradation of ATP in a ·OH-

mediated oxidation system [56]. Therefore, the significant retardation effect of chloride ions on ATP degradation in the cathode is likely due to their interaction with the electrode surfaces, which influences the electrocatalytic reactions. The modest enhancement of SMX degradation by chloride ions can be attributed to the generation of reactive chlorine species. These species arise through the direct oxidation of chloride ions at the anode and their interactions with PMS [57]. Because of the presence of various inorganic ions in the river water, pollutant degradation in this water matrix was significantly slower than in deionized water (Figure 7g,h). Measures should be taken in future research to mitigate the adverse effects of these inorganic anions.

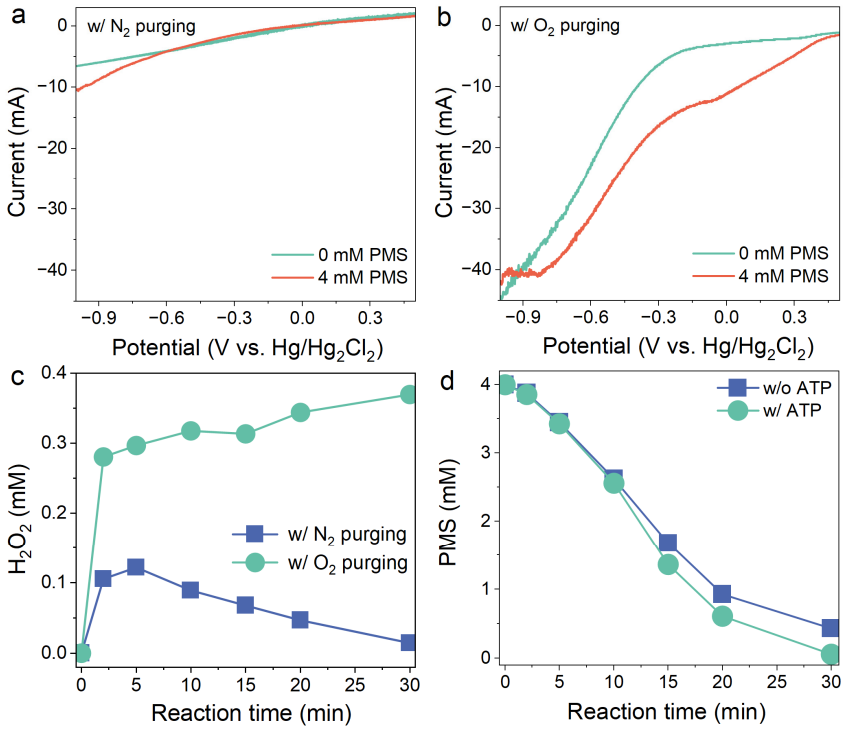


Figure 6. Linear sweep voltammetry curves of PMS-EAOP with (**a**) N_2 or (**b**) O_2 purging, and (**c**) effect of gas purging on H_2O_2 formation and (**d**) PMS decomposition in PMS-EAOP. Conditions: [PMS] = 2.5 mM, [ATP] = 5 μM, (**c**,**d**) voltage = −2 V, and initial pH = 3.2 ± 0.1.

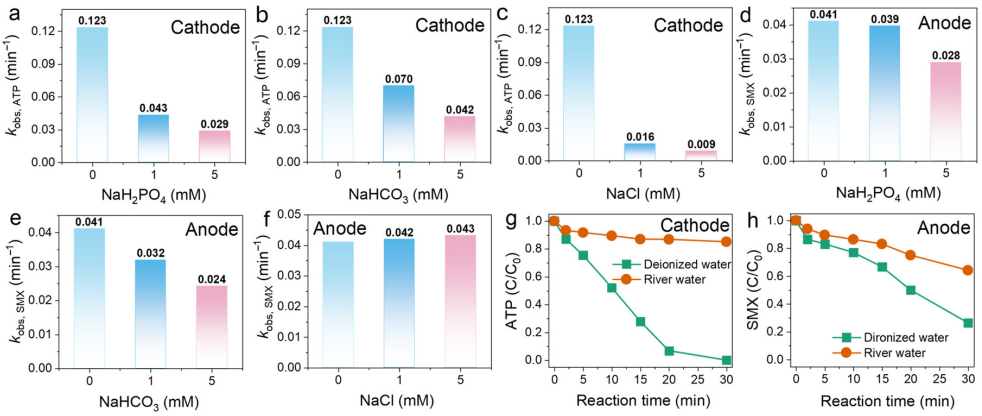


Figure 7. ATP degradation by PMS-EAOP in the presence of (**a**–**f**) different levels of anions and (**g**,**h**) water matrices. Conditions: [PMS] = 2.5 mM, [ATP] = 5 μM, [SMX] = 5 μM, voltage = −2 V, and initial pH = 3.2 ± 0.1.

4. Conclusions

This study successfully developed a PMS-EAOP by combining N-CNTs and PMS into an efficient electrocatalytic system aimed at degrading emerging contaminants. The system achieved >99% removal of ATP at the cathode within 30 min, while SMX was effectively degraded at both the cathode (>98.5%) and anode (~75.0%). Quantitative EPR analysis demonstrated that the ·OH signal intensity at the cathode was 4.8-fold higher than at the anode, confirming that cathodic PMS activation is the primary driver for recalcitrant pollutant destruction. In contrast, the anode functioned as a selective zone where SMX was removed via direct electrolysis, while ATP remained resistant (<20% removal) due to its electron-deficient substituents. Water matrix components imposed significant limitations: Chloride ions reduced the k_{obs} of ATP degradation from 0.123 to 0.009 min^{-1}, representing a 92.7% inhibition. While promising for selective decontamination, future work must address the matrix effects, the long-term structural stability of carbonaceous electrodes under high anodic potentials, and the mass transfer limitations for large-scale wastewater treatment. In addition, future studies will focus on monitoring real-time pH variations in the cathode and anode chambers and performing a comprehensive cost–benefit analysis (e.g., electrical energy consumption) to enhance the system's practical applicability.

Supplementary Materials: The following supporting information can be downloaded at https://www.mdpi.com/article/10.3390/w18030326/s1. Text S1: catalyst characterization; Text S2: electrochemical experiments and characterization; Text S3: ATP and SMX quantification; Text S4: PMS quantification; Text S5: H_2O_2 quantification; Text S6: EPR analysis; Table S1: formula and CAS numbers of chemicals used in this study; Table S2: characteristics of lake water used in this study; Table S3 [36–38]: comparison of the treatment efficacy of recently reported PMS-EAOPs with the findings of the present study; Table S4 [51–53]: equilibrium constants for phosphate and bicarbonate; Figure S1: high-resolution N 1s XPS spectrum of N-CNT2; Figure S2: electrochemical characterization; Figure S3: plots of -ln(C/C0) versus reaction time under different reaction conditions; Figure S4: EPR spectra of reaction solutions at cathode and anode of PMS-EAOP; Figure S5: standard curves for (a) PMS and (b) H_2O_2 at different concentrations.

Author Contributions: Conceptualization, Y.F.; methodology, C.Z. and Y.F.; formal analysis, C.Z.; investigation, C.Z.; resources, G.-G.Y. and J.-L.Z.; data curation, C.Z.; writing—original draft preparation, C.Z. and Y.F.; writing—review and editing, Y.F.; supervision, Y.F.; project administration, Y.F.; funding acquisition, Y.F. and J.-L.Z. All authors have read and agreed to the published version of the manuscript.

Funding: This work was supported by the National Natural Science Foundation of China (No. 42077340, 52000080), Science and Technology Project in Guangzhou, China (2024A04J6538), and Guangdong Special Support Program (No. 2024TX08A357).

Data Availability Statement: The original contributions presented in this study are included in the article/Supplementary Materials. Further inquiries can be directed to the corresponding authors.

Conflicts of Interest: The authors declare no conflicts of interest.

References

1. Morin-Crini, N.; Lichtfouse, E.; Liu, G.; Balaram, V.; Ribeiro, A.R.L.; Lu, Z.; Stock, F.; Carmona, E.; Teixeira, M.R.; Picos-Corrales, L.A. Worldwide cases of water pollution by emerging contaminants: A review. *Environ. Chem. Lett.* **2022**, *20*, 2311–2338. [CrossRef]
2. Khan, S.; Naushad, M.; Govarthanan, M.; Iqbal, J.; Alfadul, S.M. Emerging contaminants of high concern for the environment: Current trends and future research. *Environ. Res.* **2022**, *207*, 112609. [CrossRef] [PubMed]
3. Yang, Y.; Ok, Y.S.; Kim, K.-H.; Kwon, E.E.; Tsang, Y.F. Occurrences and removal of pharmaceuticals and personal care products (PPCPs) in drinking water and water/sewage treatment plants: A review. *Sci. Total Environ.* **2017**, *596–597*, 303–320. [CrossRef] [PubMed]

4. Nguyen, M.-K.; Lin, C.; Nguyen, H.-L.; Hung, N.T.Q.; La, D.D.; Nguyen, X.H.; Chang, S.W.; Chung, W.J.; Nguyen, D.D. Occurrence, fate, and potential risk of pharmaceutical pollutants in agriculture: Challenges and environmentally friendly solutions. *Sci. Total Environ.* **2023**, *899*, 165323. [CrossRef] [PubMed]
5. Tsvetkov, N.; Samson-Robert, O.; Sood, K.; Patel, H.S.; Malena, D.A.; Gajiwala, P.H.; Maciukiewicz, P.; Fournier, V.; Zayed, A. Chronic exposure to neonicotinoids reduces honey bee health near corn crops. *Science* **2017**, *356*, 1395–1397. [CrossRef]
6. Woodcock, B.A.; Bullock, J.M.; Shore, R.F.; Heard, M.S.; Pereira, M.G.; Redhead, J.; Ridding, L.; Dean, H.; Sleep, D.; Henrys, P.; et al. Country-specific effects of neonicotinoid pesticides on honey bees and wild bees. *Science* **2017**, *356*, 1393–1395. [CrossRef]
7. Phogat, A.; Singh, J.; Kumar, V.; Malik, V. Toxicity of the acetamiprid insecticide for mammals: A review. *Environ. Chem. Lett.* **2022**, *20*, 1453–1478. [CrossRef]
8. Zhao, X.; Farajtabar, A.; Zhao, H.; Han, G. Solubility and Solvent Effect of Acetamiprid in Thirteen Pure Solvents and Aqueous Solutions of Ethanol. *J. Chem. Eng. Data* **2019**, *64*, 3505–3513. [CrossRef]
9. Chen, Y.; Ling, J.; Yu, W.; Zhang, L.; Wu, R.; Yang, D.; Qu, J.; Jin, H.; Tao, Z.; Shen, Y.; et al. Identification of point and nonpoint emission sources of neonicotinoid pollution in regional surface water. *Water Res.* **2024**, *248*, 120863. [CrossRef]
10. Toumi, K.; Arbi, A.; Soudani, N.; Lomadze, A.; Haouas, D.; Bertuzzi, T.; Cardinali, A.; Lamastra, L.; Capri, E.; Suciu, N.A. Ecotoxicological Risk Assessment and Monitoring of Pesticide Residues in Soil, Surface Water, and Groundwater in Northwestern Tunisia. *Water* **2025**, *17*, 2387. [CrossRef]
11. Dominguez, J.R.; González, T.; Correia, S.E.; Núñez, M.M. Emerging Contaminants Decontamination of WWTP Effluents by BDD Anodic Oxidation: A Way towards Its Regeneration. *Water* **2023**, *15*, 1668. [CrossRef]
12. Lucas, M.S.; Teixeira, A.R.; Jorge, N.; Peres, J.A. Industrial Wastewater Treatment by Coagulation–Flocculation and Advanced Oxidation Processes: A Review. *Water* **2025**, *17*, 1934. [CrossRef]
13. Lee, J.; von Gunten, U.; Kim, J.H. Persulfate-based advanced oxidation: Critical assessment of opportunities and roadblocks. *Environ. Sci. Technol.* **2020**, *54*, 3064. [CrossRef] [PubMed]
14. Wang, J.; Wang, S. Activation of persulfate (PS) and peroxymonosulfate (PMS) and application for the degradation of emerging contaminants. *Chem. Eng. J.* **2018**, *334*, 1502–1517. [CrossRef]
15. Lei, Z.; Ma, J.; Cao, Y.; Zhang, M.; Zuo, Q.; Li, M.; Liu, Y.; Wan, P.; Dai, L. Co-nZVI@ATP activated persulfate for the degradation of Bisphenol S: Treatment efficiency and mechanism. *Environ. Res.* **2025**, *285*, 122603. [CrossRef]
16. Martínez-Huitle, C.A.; Panizza, M. Electrochemical oxidation of organic pollutants for wastewater treatment. *Curr. Opin. Electrochem.* **2018**, *11*, 62–71. [CrossRef]
17. Gong, C.; Han, J.; He, C.; Shi, L.; Shan, Y.; Zhang, Z.; Wang, L.; Ren, X. Insights into degradation of pharmaceutical pollutant atenolol via electrochemical advanced oxidation processes with modified Ti4O7 electrode: Efficiency, stability and mechanism. *Environ. Res.* **2023**, *228*, 115920. [CrossRef]
18. Moreira, F.C.; Boaventura, R.A.R.; Brillas, E.; Vilar, V.J.P. Electrochemical advanced oxidation processes: A review on their application to synthetic and real wastewaters. *Appl. Catal. B Environ.* **2017**, *202*, 217–261. [CrossRef]
19. Heidari, Z.; Pelalak, R.; Zhou, M. A critical review on the recent progress in application of electro-Fenton process for decontamination of wastewater at near-neutral pH. *Chem. Eng. J.* **2023**, *474*, 145741. [CrossRef]
20. Deng, F.; Olvera-Vargas, H.; Zhou, M.; Qiu, S.; Sirés, I.; Brillas, E. Critical Review on the Mechanisms of Fe2+ Regeneration in the Electro-Fenton Process: Fundamentals and Boosting Strategies. *Chem. Rev.* **2023**, *123*, 4635–4662. [CrossRef]
21. Lim, H.J.; Kim, D.J.; Rigby, K.; Chen, W.; Xu, H.; Wu, X.; Kim, J.-H. Peroxymonosulfate-Based Electrochemical Advanced Oxidation: Complication by Oxygen Reduction Reaction. *Environ. Sci. Technol.* **2023**, *57*, 19054–19063. [CrossRef]
22. Deng, H.; Li, Q.; Liu, J.; Wang, F. Active sites for oxygen reduction reaction on nitrogen-doped carbon nanotubes derived from polyaniline. *Carbon* **2017**, *112*, 219–229. [CrossRef]
23. Niu, W.-J.; Wang, Y.-P.; He, J.-Z.; Liu, W.-W.; Liu, M.-C.; Shan, D.; Lee, L.; Chueh, Y.-L. Highly stable nitrogen-doped carbon nanotubes derived from carbon dots and metal-organic frameworks toward excellent efficient electrocatalyst for oxygen reduction reaction. *Nano Energy* **2019**, *63*, 103788. [CrossRef]
24. Ning, X.; Li, Y.; Ming, J.; Wang, Q.; Wang, H.; Cao, Y.; Peng, F.; Yang, Y.; Yu, H. Electronic synergism of pyridinic-and graphitic-nitrogen on N-doped carbons for the oxygen reduction reaction. *Chem. Sci.* **2019**, *10*, 1589–1596. [CrossRef] [PubMed]
25. Soni, S.K.; Thomas, B.; Thomas, S.B.; Tile, P.S.; Sakharwade, S.G. Carbon nanotubes as exceptional nanofillers in polymer and polymer/fiber nanocomposites: An extensive review. *Mater. Today Commun.* **2023**, *37*, 107358. [CrossRef]
26. Guo, R.; Bi, Z.; Xi, B.; Guo, C.; Zhang, H.; Lv, N.; Hu, G.; Xu, J. A new generation pathway of singlet oxygen in heterogeneous single–atom Mn catalyst/peroxymonosulfate system. *Chem. Eng. J.* **2024**, *481*, 148629. [CrossRef]
27. Takeyasu, K.; Furukawa, M.; Shimoyama, Y.; Singh, S.K.; Nakamura, J. Role of Pyridinic Nitrogen in the Mechanism of the Oxygen Reduction Reaction on Carbon Electrocatalysts. *Angew. Chem. Int. Ed.* **2021**, *60*, 5121–5124. [CrossRef]
28. Ma, C.; Fang, X.; Jiang, S.; Li, F.; Liu, Y. Enhanced electro-peroxymonosulfate activation using a carbon nanotube filter with a functionalized polyelectrolyte. *Environ. Sci. Water Res. Technol.* **2022**, *8*, 2314–2325. [CrossRef]

29. Du, X.; Xie, W.; Long, X.; Li, D.; Huang, W.; Zhang, I.Y.; Huang, R. Efficient Removal of Sulfamethoxazole in Electro-Oxidation System with Boron-Doped Diamond Anode and Electrolyte NaCl: Degradation Mechanisms. *Molecules* **2025**, *30*, 1056. [CrossRef]
30. Liang, Y.; Yang, K.; Zhang, X.; He, W.; Kong, X.; Zhou, Y.; Ma, J. Voltage-confined flow-through anodic oxidation enables efficient pollutant removal and no chlorinated byproducts formation. *Sep. Purif. Technol.* **2025**, *355*, 129704. [CrossRef]
31. Liu, T.; Zhang, D.; Yin, K.; Yang, C.; Luo, S.; Crittenden, J.C. Degradation of thiacloprid via unactivated peroxymonosulfate: The overlooked singlet oxygen oxidation. *Chem. Eng. J.* **2020**, *388*, 124264. [CrossRef]
32. Tian, Y.; Hai, R.; Liu, Y.; Nie, D.; Lu, Y.; Zhu, H.; Yang, X. Zn-Driven AgI Anchoring on Ti-MOF for Photocatalytic Singlet Oxygen Generation in Imidacloprid Removal. *ACS Appl. Mater. Interfaces* **2025**, *17*, 30988–30999. [CrossRef] [PubMed]
33. Guan, Y.H.; Ma, J.; Li, X.C.; Fang, J.Y.; Chen, L.W. Influence of pH on the formation of sulfate and hydroxyl radicals in the UV/Peroxymonosulfate system. *Environ. Sci. Technol.* **2011**, *45*, 9308–9314. [CrossRef] [PubMed]
34. Zhang, T.; Zhu, H.; Croué, J.-P. Production of sulfate radical from peroxymonosulfate induced by a magnetically separable $CuFe_2O_4$ spinel in water: Efficiency, stability, and mechanism. *Environ. Sci. Technol.* **2013**, *47*, 2784–2791. [CrossRef] [PubMed]
35. Hieu Nhu, H.D.; Tri, D.V.; Luu, T.L.; Trippel, J.; Wagner, M. Degradation of 29 per- and poly-fluoroalkyl substances (PFAS) in water using fenton-assisted electrochemical oxidation process. *Sep. Purif. Technol.* **2025**, *362*, 131908. [CrossRef]
36. Xu, Y.; Li, W.; Wang, J.; Wu, D.; Li, N.; Li, Y.; Fan, X.; Peng, W. Activation potential decreasing of iron oxide/graphite felt cathode by introducing Mn in electrochemical Fenton-like reactions. *Chemosphere* **2024**, *369*, 143885. [CrossRef]
37. Jing, J.; Wang, X.; Zhou, M. Electro-enhanced activation of peroxymonosulfate by a novel perovskite-Ti4O7 composite anode with ultra-high efficiency and low energy consumption: The generation and dominant role of singlet oxygen. *Water Res.* **2023**, *232*, 119682. [CrossRef]
38. He, J.; Yang, Y.; Hong, P.; Li, Y.; Xie, C.; Wu, Z.; Li, M.; Kong, L. Oxygen Vacancies of Mn/CeOx-H induced non-radical activation of peroxymonosulfate through electron mediation for bisphenol A degradation. *J. Environ. Chem. Eng.* **2023**, *11*, 111078. [CrossRef]
39. Zong, Y.; Guan, X.; Xu, J.; Feng, Y.; Mao, Y.; Xu, L.; Chu, H.; Wu, D. Unraveling the Overlooked Involvement of High-Valent Cobalt-Oxo Species Generated from the Cobalt(II)-Activated Peroxymonosulfate Process. *Environ. Sci. Technol.* **2020**, *54*, 16231–16239. [CrossRef]
40. Chen, T.; Zhang, G.; Sun, H.; Hua, Y.; Yang, S.; Zhou, D.; Di, H.; Xiong, Y.; Hou, S.; Xu, H.; et al. Robust Fe-N4-C6O2 single atom sites for efficient PMS activation and enhanced FeIV = O reactivity. *Nat. Commun.* **2025**, *16*, 2402. [CrossRef]
41. Gao, H.-Y.; Huang, C.-H.; Mao, L.; Shao, B.; Shao, J.; Yan, Z.-Y.; Tang, M.; Zhu, B.-Z. First Direct and Unequivocal Electron Spin Resonance Spin-Trapping Evidence for pH-Dependent Production of Hydroxyl Radicals from Sulfate Radicals. *Environ. Sci. Technol.* **2020**, *54*, 14046–14056. [CrossRef] [PubMed]
42. Dell'Arciprete, M.L.; Santos-Juanes, L.; Sanz, A.A.; Vicente, R.; Amat, A.M.; Furlong, J.P.; Mártire, D.O.; Gonzalez, M.C. Reactivity of hydroxyl radicals with neonicotinoid insecticides: Mechanism and changes in toxicity. *Photochem. Photobiol. Sci.* **2009**, *8*, 1016–1023. [CrossRef]
43. Dell'Arciprete, M.L.; Cobos, C.J.; Mártire, D.O.; Furlong, J.P.; Gonzalez, M.C. Reaction kinetics and mechanisms of neonicotinoid pesticides with sulfate radicals. *New J. Chem.* **2011**, *35*, 672–680. [CrossRef]
44. Neta, P.; Huie, R.E.; Ross, A.B. Rate constants for reactions of inorganic radicals in aqueous solution. *J. Phys. Chem. Ref. Data* **1988**, *17*, 1027–1284. [CrossRef]
45. Buxton, G.V.; Greenstock, C.L.; Helman, W.P.; Ross, A.B. Critical review of rate constants for reactions of hydrated electrons, hydrogen atoms and hydroxyl radicals ($\cdot OH/\cdot O^-$) in aqueous solution. *J. Phys. Chem. Ref. Data* **1988**, *17*, 513–886. [CrossRef]
46. Chawla, O.P.; Fessenden, R.W. Electron spin resonance and pulse radiolysis studies of some reactions of peroxysulfate (SO4.1,2). *J. Phys. Chem.* **1975**, *79*, 2693–2700. [CrossRef]
47. Panizza, M.; Cerisola, G. Direct And Mediated Anodic Oxidation of Organic Pollutants. *Chem. Rev.* **2009**, *109*, 6541–6569. [CrossRef]
48. Zhao, B.; Li, Y.; Tian, Y.; Ying, G.-G.; Zhong, J.; Wu, D.; Feng, Y. Revealing the mechanism of singlet oxygen formation during the activation of Peroxymonosulfate by Feco dual-atom catalysts. *Sep. Purif. Technol.* **2026**, *381*, 135590. [CrossRef]
49. Zhang, Y.; Kang, W.; Yu, H.; Chen, S.; Quan, X. Electrochemical activation of peroxymonosulfate in cathodic micro-channels for effective degradation of organic pollutants in wastewater. *J. Hazard. Mater.* **2020**, *398*, 122879. [CrossRef]
50. Lu, Z.; Chen, G.; Siahrostami, S.; Chen, Z.; Liu, K.; Xie, J.; Liao, L.; Wu, T.; Lin, D.; Liu, Y.; et al. High-efficiency oxygen reduction to hydrogen peroxide catalysed by oxidized carbon materials. *Nat. Catal.* **2018**, *1*, 156–162. [CrossRef]
51. Czapski, G.; Lymar, S.V.; Schwarz, H.A. Acidity of the Carbonate Radical. *J. Phys. Chem. A* **1999**, *103*, 3447–3450. [CrossRef]
52. Marcandalli, G.; Villalba, M.; Koper, M.T.M. The Importance of Acid–Base Equilibria in Bicarbonate Electrolytes for CO2 Electrochemical Reduction and CO Reoxidation Studied on Au(hkl) Electrodes. *Langmuir* **2021**, *37*, 5707–5716. [CrossRef]
53. Li, N.; Wang, Y.; Cheng, X.; Dai, H.; Yan, B.; Chen, G.; Wang, S. Influences and mechanisms of phosphate ions onto persulfate activation and organic degradation in water treatment: A review. *Water Res.* **2022**, *222*, 118896. [CrossRef]
54. Maruthamuthu, P.; Neta, P. Phosphate radicals. Spectra, acid-base equilibriums, and reactions with inorganic compounds. *J. Phys. Chem.* **1978**, *82*, 710–713. [CrossRef]

55. Lente, G.; Kalmár, J.; Baranyai, Z.; Kun, A.; Kék, I.; Bajusz, D.; Takács, M.; Veres, L.; Fábián, I. One- Versus Two-Electron Oxidation with Peroxomonosulfate Ion: Reactions with Iron(II), Vanadium(IV), Halide Ions, and Photoreaction with Cerium(III). *Inorg. Chem.* **2009**, *48*, 1763–1773. [CrossRef]
56. Pinto, M.I.; Salgado, R.; Laia, C.A.T.; Cooper, W.J.; Sontag, G.; Burrows, H.D.; Branco, L.; Vale, C.; Noronha, J.P. The effect of chloride ions and organic matter on the photodegradation of acetamiprid in saline waters. *J. Photochem. Photobiol. A Chem.* **2018**, *360*, 117–124. [CrossRef]
57. Wang, C.; Yin, L.; Xu, Z.; Niu, J.; Hou, L.-A. Electrochemical degradation of enrofloxacin by lead dioxide anode: Kinetics, mechanism and toxicity evaluation. *Chem. Eng. J.* **2017**, *326*, 911–920. [CrossRef]

Disclaimer/Publisher's Note: The statements, opinions and data contained in all publications are solely those of the individual author(s) and contributor(s) and not of MDPI and/or the editor(s). MDPI and/or the editor(s) disclaim responsibility for any injury to people or property resulting from any ideas, methods, instructions or products referred to in the content.